Published in final edited form as:
J Magn Reson. 2010 February ; 202(2): 155. doi:10.1016/j.jmr.2009.10.012.

Simultaneous determination of labile proton concentration and exchange rate utilizing optimal RF power: radio frequency power (RFP) dependence of chemical exchange saturation transfer (CEST) MRI

Phillip Zhe Sun*

*Athinoula A. Martinos Center for Biomedical Imaging, Department of Radiology, Massachusetts General Hospital and Harvard Medical School, Charlestown, MA 02129

Abstract

Chemical exchange saturation transfer (CEST) MRI is increasingly used to probe mobile proteins and microenvironment properties, and shows great promise for tumor and stroke diagnosis. However, CEST MRI contrast mechanism is complex, depending not only on the CEST agent concentration, exchange and relaxation properties, but also varying with experimental conditions such as magnetic field strength and RF power. Hence, it remains somewhat difficult to quantify apparent CEST MRI contrast for properties such as pH, temperature and protein content. In particular, CEST MRI is susceptible to RF spillover effects in that RF irradiation may directly saturate the bulk water MR signal, leading to an optimal RF power at which the CEST contrast is maximal. Whereas RF spillover is generally considered an adverse effect, it is noted here that the optimal RF power strongly varies with exchange rate, although with negligible dependence on labile proton concentration. An empirical solution suggested that optimal RF power may serve as a sensitive parameter for simultaneously determining the labile proton content and exchange rate, hence, allowing improved characterization of the CEST system. The empirical solution was confirmed by numerical simulation, and experimental validation is needed to further evaluate the proposed technique.

Keywords

amide proton transfer (APT); chemical exchange saturation transfer (CEST)

1. INTRODUCTION

Chemical exchange saturation transfer (CEST) MRI is increasingly used to detect dilute proteins via the interaction between protein labile groups and bulk water protons [1–7]. Because saturation transfer confers sizable sensitivity enhancement to CEST MRI, it has recently been applied to measure metabolites and byproducts such as glucose, glycogen, and lactate as well

*Corresponding author: Phillip Zhe Sun, PhD, Athinoula A. Martinos Center for Biomedical Imaging, Department of Radiology, Massachusetts General Hospital, Harvard Medical School, Rm 2301,149 13th street, Charlestown, MA 02129, pzhesun@nmr.mgh.harvard.edu, Phone: 617-726-4060 Fax: 617-726-7422.

as enzymes and viruses, and holds great promise for *in vivo* translation [4;8–13]. In addition, cells transfected with genes encoding polypeptide CEST agents can be detected both *in vitro* and *in vivo*, making CEST MRI a viable alternative to commonly used paramagnetic iron oxide-based cell tracking methods [10;14–19].Moreover, amide proton transfer (APT) imaging, a variant of CEST MRI that specifically probes labile amide protons, has been explored for imaging diseases such as acute stroke and tumor, and is currently under intensive evaluation for clinical translation [20–22]. Once fully developed, CEST MRI has great potential to augment conventional MRI methods for a broad range of pre-clinical and clinical applications.

Because CEST MRI contrast depends on not only the chemical exchange rate of labile groups, but also their concentration, it is useful to develop a quantitative CEST MRI technique that can simultaneously estimate the concentration and exchange properties of CEST agents. Such a technique may be very useful for *in vivo* imaging, particularly when severe tissue heterogeneity is present. Toward this goal, ratiometric CEST MRI has been proposed, taking advantage of the unequal pH-dependent chemical exchange behavior of multiple labile groups so that microenvironment properties can be estimated independent of the concentration of CEST agents [23;24]. However, given that commonly used CEST agents either have a single dominant labile group, or are not well characterized for multiple exchangeable groups, there is considerable need to explore approaches complementary to ratiometric CEST MRI. This is important because experimentally obtainable CEST contrast is complex, depending on not only properties of the CEST agent such as concentration, exchange rate, chemical offset, and relaxation rate but also on experimental parameters including magnetic field strength, RF power, scheme, and duration [25–28]. For *in vivo* CEST imaging, where the labile proton concentration and microenvironment properties may be dynamic and heterogeneous, there is particularly strong need for a quantitative CEST MRI technique [9;29–31]. It is in fact very helpful to go one step further from the apparent CEST MRI contrast (magnetization transfer asymmetry) to derive underlying parameters and improve our mechanistic understanding of tissue pathophysiology, as in cases of stroke and tumor. For instance, brain tumor is heterogeneous and often involves various pathological transformations including edema, acidification, change in protein composition and content as well as abnormal vasculature formation [20;32]. It is hence helpful to fully develop *in vivo* CEST MRI to guide therapy [33].

Our study aims to develop a relatively simplified yet practical approach for simultaneous estimation of both labile proton concentration and exchange properties. It is known that CEST MRI is susceptible to direct RF saturation (spillover) effect as the bulk water MR signal may decrease as a result of off-resonance RF irradiation, independent of the saturation transfer phenomenon. In fact, experiments have shown that CEST contrast initially increases with RF power, but plateaus and subsequently decreases at higher RF power, suggesting RF spillover effects. As such, for a given CEST system, there is an optimal RF power that maximizes the experimentally obtainable contrast, at which point saturation of labile protons and RF spillover effects are comparable. In fact, both numerical simulation and empirical solution methods have been developed to elucidate the CEST MRI contrast mechanism [26;29;34]. Because the spillover effect reduces the sensitivity and specificity of CEST MRI, it has been generally considered an adverse effect. However, we postulate that additional insight can be gained by probing the radio frequency power (RFP) - dependent nature of the CEST MRI contrast. In this study, we investigated the dependence of optimal RF power on the concentration and exchange properties of CEST agents, as well as chemical offset and relaxation parameters. Our results showed that optimal RF power varies strongly with the chemical exchange rate while it has negligible dependence on labile proton content. To test the hypothesis, CEST MRI was numerically simulated using the classic 2-pool exchange model, and the results confirmed our theoretical prediction [34]. As such, we identified an experimentally measureable parameter capable of simultaneously deriving exchange rate and labile proton concentration, hence,

complementing the commonly used apparent CEST MRI technique. We also evaluated the sensitivity of optimal RF power to chemical offset and relaxation rates to gain further insight about the practicability of the proposed RFP-CEST MRI technique.

2. THEORY

The steady state CEST ratio (CESTR) is often given by MT ratio (MTR) asymmetry, which can be described by an empirical solution as [26;29]:

$$\mathrm{CESTR}=\frac{f\cdot k_{sw}}{R_{1w}+f\cdot k_{sw}}\cdot\alpha\cdot(1-\sigma) \tag{1}$$

where α is the labeling coefficient, σ is the spillover factor, k_{sw} is the chemical exchange rate from labile protons to bulk water, f is labile proton concentration with respect to bulk water proton, and R_{1w} is bulk water longitudinal relaxation rate [28;35]. This solution (Eq. 1) was derived empirically by combining two solutions; one for weak RF power when RF spillover effect is negligible $\left(\text{i.e., CESTR}=\frac{f\cdot k_{sw}}{R_{1w}+f\cdot k_{sw}}\cdot\alpha\right)$ and another one for strong RF power $\left(\text{i.e., CESTR}=\frac{f\cdot k_{sw}}{R_{1w}+f\cdot k_{sw}}\cdot(1-\sigma)\right)$, in which labile protons are fully saturated [26;35;36]. Although it is not a direct solution from the 2-pool model, the empirical solution has been shown to agree reasonably well with numerically simulated results for slow and intermediate chemical exchange processes [26]. Specifically, the labeling coefficient is given by $\frac{\omega_1^2}{p\cdot q+\omega_1^2}$, where ω_1 is the RF power, $p=r_{2s}-\frac{k_{sw}k_{ws}}{r_{2w}}$ and $q=r_{1s}-\frac{k_{sw}k_{ws}}{r_{1w}}$, in which $k_{ws}=f\cdot k_{sw}$. Moreover, $r_{1w,s}$ and $r_{2w,s}$ are the apparent relaxation rates, given by $r_{1w,s}=R_{1w,s}+k_{ws,sw}$ and $r_{2w,s}=R_{2w,s}+k_{ws,sw}$, respectively. The spillover factor is equal to $1-\frac{r_{1w}}{k_{ws}}\left(\frac{R_{1w}r_{zs}\cos^2\theta+R_{1s}k_{ws}\cos\theta\cos^2(\theta/2)}{r_{zw}r_{zs}-k_{ws}k_{sw}\cos^2(\theta/2)}-\frac{R_{1w}r_{2s}\cos^2\theta}{r_{zw}r_{2s}-k_{ws}k_{sw}\sin^2\theta}\right)$, where $r_{zw}=r_{1w}\cos^2\theta/2+r_{2w}\sin^2\theta/2$, $r_{zs}=r_{1s}\cos^2\theta+r_{2s}\sin^2\theta$ and $\theta=\tan^{-1}(\omega_1/\Delta\omega_s)$.

The optimal RF power can be obtained by nulling the first order derivative of Eq. 1 against RF power, and has been shown to be equal to [26],

$$\omega_{1\_\mathrm{opt}}=\sqrt{pq\left\{\sqrt{1+\frac{4(f_s+f_w)(1-\beta)\eta_{2s}}{\left[\begin{array}{l}f_s\eta_{2s}(1+2(1-\beta)+\eta_s+4\eta_w)+\\ f_w(4+4\beta^2+\eta_{2s}(5+\eta_{2s}+8\eta_w)-4\beta(2+\eta_{2s}+\eta_{2s}\eta_w))\end{array}\right]}\frac{\Delta\omega^2}{p\cdot q}}-1\right\}} \tag{2}$$

where $\beta=\frac{k_{ws}k_{sw}}{r_{1w}r_{1s}}$, $\eta_w=\frac{R_{2w}-R_{1w}}{r_{1w}}$, $\eta_s=\frac{R_{2s}-R_{1s}}{r_{1s}}$, $\eta_{2s}=\frac{r_{2s}}{r_{1s}}$, $f_w=\frac{R_{1w}}{r_{1w}}$, and $f_s=\frac{R_{1s}}{k_{sw}}$. Nevertheless, this optimal RF power solution is complex, and numerical simulation is necessary in order to gain some helpful insights about the properties of optimal RF power, in particular, its dependence on labile proton concentration and chemical exchange rate.

3. METHODS

NUMERICAL SIMULATION

CEST MRI was numerically simulated using the classic 2-pool exchange model in Matlab 7.4 (Mathworks, Natick MA), as reported previously [25;26;34]. We examined the dependence of optimal RF power on CEST agent's properties by simulating CEST MRI contrast as a function of RF irradiation power for representative ranges of labile proton concentration and exchange rate. Considering the specific absorption rate (SAR) limit, RF power was simulated between 0 and 3 μT (~130 Hz). A chemical offset of 700 Hz was chosen for simulation as it represents the frequency offset of ensemble amide proton from endogenous proteins and peptides, observed at 4.7T. Typical longitudinal and transverse relaxation times for bulk water and labile proton pools were used, being 1.5 s, 1 s, 60 ms and 10 ms, respectively, which are similar to relaxation times found by *in vivo* observation and tissue-like gel phantom [28;29]. In addition, our current study investigated long continuous wave (CW) RF irradiation, and only steady state CEST MRI contrast was simulated.

1) Chemical exchange rate and labile proton concentration dependence—In this work, we studied slow to intermediate exchange rates between 1 and 150 s^{-1}, and varied the labile proton concentration with respect to bulk water proton from 1:2000 to 1:500. Specifically, labile proton concentration was assumed to be 1:1000 when evaluating chemical exchange rate effect, while the exchange rate was set to be 75 s^{-1} when labile proton concentration effect was investigated. For a given set of labile proton concentration and exchange rate, the optimal RF power was determined by finding the RF power that maximizes CEST MRI contrast.

2) Chemical offset dependence—We assessed how chemical offset may affect optimal RF power. Specifically, three representative chemical offsets, 450, 700 and 1400 Hz, which correspond to the chemical offset of endogenous amide protons (3.5 ppm from the bulk water resonance) at magnetic field strengths of 3, 4.7 and 9.4 T, respectively, were simulated. Same exchange rate and labile proton concentration were simulated (i.e., f=1:1000 when exchange rate effect is evaluated or k_{sw}=75 s^{-1} when labile proton concentration effect is studied).

3) Relaxation time dependence—We also studied how optimal RF power may depend on relaxation rates of bulk water and labile species. Specifically, three bulk water T_{1w} constants of 1,1.5 and 2 s were evaluated with T_{2w} kept at 60 ms. In addition, simulation was repeated for three bulk water T_{2W} times, being 40, 60 and 100 ms for a T_{1w} of 1.5 s. Moreover, three labile proton T_{1s} were tested, being 1, 1.5 and 2 s while bulk water relaxation parameters T_{1w} and T_{2W} were assumed to be 1.5 s and 60 ms, respectively, and T_{2s} was 10 ms. Furthermore, labile proton transverse relaxation time T_{2s} effect was studied by simulating three representative values, being 10, 15 and 20 ms, for the same bulk water relaxation rates and T_{1s} of 1 s.

We also tested whether the exchange rate and labile proton concentration can be derived from the optimal RF power. In this study, relaxation rates were assumed to be known, which is reasonable as they may be measured directly or pre-determined from numerical fitting. Only two variables are assumed to be unknown, exchange rate (k_{sw}) and labile proton concentration (f). Specifically, exchange rate was first estimated from optimal RF power using Eq. 2 by deriving the exchange rate, whose corresponding optimal RF power is equal to the simulated value. Labile proton concentration can be subsequently calculated from the derived exchange rate and CEST MRI contrast from Eq. 1. A schematic flow chart is shown in Fig. 4 to describe this Procedure.

4. RESULTS

Fig. 1 illustrates two 2-pool exchange models with different exchange rate and labile proton concentration. Specifically, Fig. 1 a shows concentrated CEST agents undergoing slow chemical exchange with bulk water; while Fig. 1 b represents the counter scenario where dilute CEST agents undergoing faster chemical exchange with bulk water. Our study aims to investigate whether exchange rate and labile proton concentration can be simultaneously determined by CEST MRI, hence, develops more quantitative CEST MRI.

Fig. 2 shows how CEST MRI contrast varies with RF power when exchange rate and labile proton concentration is varied by comparing the empirical solution with numerical simulation. Fig. 2 a shows CEST MRI contrast for three representative exchange rates, 30 (up triangle), 75 (down triangle) and 150 (square) s^{-1}, for a representative concentration of 1:1000. It is important to note that empirical solution (solid lines) overlapped with numerical simulation, indicating that although not directly derived from 2-pool exchange model, the empirical solution is sufficiently accurate to describe slow and intermediate chemical exchange processes. The CEST MRI contrast initially increases with RF power, while it decreases when RF power is too strong, leading to an optimal RF power at which CEST MRI contrast reaches maxima. The optimal RF power was extrapolated and shown in dashed line. In addition, the optimal RF power is plotted as a function of exchange rate in Fig. 2b, with circles, solid line and dash dotted line represent numerical simulation, solution from Eq. 1 and estimation from Eq. 2, respectively, which are all in good agreement. It shows that the optimal RF power strongly varies with chemical exchange rate. In addition, zig-zag behavior of optimal RF power was observed, which can attributed to finite step increase of RF power in numerical simulation. Specifically, RF power was varied 0.06 μT per step, and for a narrow range of exchange rate, optimal RF power becomes undistinguishable within 0.06 μT. In contrast, Fig. 2 c depicts the RF power dependence of CEST contrast as a function of labile proton concentration. Three representative concentrations of 1:2000 (up triangle), 1:1000 (down triangle), and 1:500 (square) were simulated, for a representative exchange rate of 75 s^{-1}. The optimal RF power (dashed line) was overlaid in Fig. 2c. The optimal RF power is plotted as a function of labile proton concentration in Fig. 2 d, which showed that the optimal RF power remains the same despite four folds increase in labile proton concentration.

CEST MRI contrast, however, is very complex. It depends on not only exchange rate and labile proton concentration; it also varies with chemical offset and relaxation parameters. Thereby, it is important to elucidate how such factors affect optimal RF power. Specifically, three representative chemical offsets of 450, 700 and 1400 Hz were explored, which correspond to amide proton offset of endogenous cerebral proteins/peptides (3.5 ppm) at field strengths of 3, 4.7 and 9.4 Tesla, respectively (Figs. 3 a and b). It shows that change of chemical offset did not alter the finding that optimal RF power strongly depends on exchange rate, while nearly independent of labile proton concentration. The observation that optimal RF power increases with chemical offset for both cases can be attributed to the fact that spillover effect is smaller at larger chemical offset, hence, resulting in an increase in the optimal RF power. In fact, for the same range of exchange rates, the increase in optimal RF power confers a broader dynamic range of optimal RF power for experimental test. In addition, CEST MRI contrast was simulated for three representative bulk water T_{1w} of 1, 1.5 and 2s, while its T_{2w} was kept at 60 ms (Figs. 3 c and d). The optimal RF power decreases at longer T_{1w}, consistent with the finding that less RF power is needed to compete with slower longitudinal relaxation. Moreover, bulk water T_{2w} effect was also evaluated by varying T_{2w} from 100, 60 and 40 ms, for a T_{1w} of 1.5 s (Figs 3 e and f). The result showed that optimal RF power is larger at longer T_{2w}, which can be attributed to less spillover effects when bulk water spectrum is relatively sharp. Moreover, RFP CEST MRI was also studied as a function of labile proton relaxation time. Because our study investigates long CW RF irradiation, very little change was observed for

three T_{1s} of 1, 1.5 and 2 s (data not shown). Similarly, optimal RF power had minimally dependence on labile proton relaxation rates when three T_{2s} of 20, 15 and 10 ms were evaluated (data not shown). As such, our results showed that although optimal RF power varies with chemical offset and to a far lesser extent, relaxation parameters, the dependence of optimal RF power upon exchange rate and labile proton concentration remains the same (i.e., optimal RF power increases with exchange rate but is nearly independent of labile proton concentration).

Our results suggested that optimal RF power is sensitive to chemical exchange rate, while nearly independent of labile proton concentration. As such, optimal RF power may serve as a sensitive parameter that allows quantification of CEST system. Specifically, chemical exchange rate may be first estimated from optimal RF power by finding the exchange rate, whose corresponding optimal RF power is equal to the derived optimal RF power following Eq. 2. Labile proton concentration can then be estimated by the empirical solution (Eq. 1). A flow chart of the proposed CEST quantification procedure is shown in Fig. 4.

We further tested whether labile proton concentration and exchange rate can be simultaneously determined by the proposed technique. Two CEST systems were examined. In the first case, chemical exchange rate was varied at a fixed labile proton concentration, while for the second case, labile proton concentration effect was studied for a given exchange rate. Specifically, for the first case, labile proton concentration was assumed to be 1:1000, while the exchange rate was varied from 1 to 150 s^{-1}, mimicking dominant pH change. As suggested in the flow chart (Fig. 4), exchange rate was first derived from optimal RF power, and labile proton concentration was subsequently calculated based on CEST MRI contrast and the derived exchange rate. Figs. 5 a and b showed exchange rate and labile proton concentration estimated from RFP CEST MRI, respectively, for the first case of dominant difference in chemical exchange rate. The derived exchange rate (k_{sw_RFP}) closely correlated with simulated exchange, and can be described by a linear function, $k_{sw\_RFP}=1.47\ k_{sw} - 9.46$ (Fig. 5a, dash dotted line). While adding a quadratic term seemed to better represent the data, with $k_{sw\_RFP}=0.0027\ k_{sw}^2 +1.06\ k_{sw} + 0.83$ (Fig. 5a, dash line), the linear fitting provided reasonable description of the results. In addition, the labile proton content was found to be 1:1175 ± 103, in comparison to the simulated value of 1:1000 (Fig. 5b). For the second case, the labile proton concentration was varied from 1:2000 to 1:500 for a representative chemical exchange rate of 75 s^{-1}, representing the scenario of dominant change in CEST agent concentration. We followed the same procedure as shown in Fig. 4. The optimal power was found to be 0.98 μT, which corresponds to a chemical exchange rate of $k_{sw\_RFP}=98\ s^{-1}$, for the simulated exchange rate of 75 s^{-1}. The labile proton concentration was then derived as $f_{RFP}=0.82$ f. In sum, numerical simulation confirmed our theoretical derivation and showed that the CEST MRI system can be reasonably characterized by probing RF power dependence of CEST MRI, in particular, the optimal RF power. Future experimental evaluation of the proposed quantitative CEST MRI technique is needed to test its practicability and sensitivity, prior to its routine use.

5. DISCUSSION

Our study showed that by elucidating the RF power dependence of CEST MRI, exchange rate and labile proton content can be simultaneously determined. Whereas RF spillover effect has been conventionally regarded an adverse effect, our work suggested that it may serve to our advantage and complement the commonly used apparent CEST MRI contrast [26;29]. The reason that optimal RF power may be a particularly sensitive parameter is because it is experimentally measurable and the tipping point for CEST MRI to transit from a regime dominated by saturation transfer enhancement to one dominated by concomitant RF spillover. In addition, if the typical dynamic range of exchange rates is known, it may be feasible to conduct CEST MRI with RF powers just about the expected optimal RF power, which saves

scan time, making the proposed technique practical [21]. In addition, the fact that exchange rate and labile proton concentration can be simultaneously derived, in reasonable agreement with numerical simulation, strongly suggests that RFP CEST MRI may serve as a quantitative CEST MRI method, warranting further evaluation. If validated, RFP CEST MRI can provide useful insights into complex and heterogeneous pathology subsequent to disease onset, including tissue pH, protein composition and content change — measurements beyond the capabilities of conventional relaxation-based MRI techniques [31].

Given the tremendous interest in ratiometric CEST imaging, it is necessary to make a brief comparison between these two quantitative techniques. Ratiometric CEST MRI relies on the principle that if chemical exchange rate of multiple labile groups respond differently to microenvironment property change, for instance, pH, the property can be estimated by comparing the relative CEST MRI change when different labile group is irradiated, independent of labile proton content [23;24]. While extremely useful, the ratiometric CEST MRI requires CEST agents to have multiple labile groups, whose chemical exchange properties have to be well calibrated and respond differently to microenvironment properties of interest. By contrast, RFP CEST MRI method can be applied for even just a single labile group. It will be interesting to see whether ratiometric and RFP CEST MRI techniques can be integrated for improved sensitivity and precision. In fact, the challenge of simultaneous assessment of contrast agent content and relaxivity is not unique to CEST MRI; it has also been a topic in the field of “smart” contrast agent development. For smart MRI probes, their relaxivity properties vary with specific changes such as pH, presence of targeted protein and enzyme to enable imaging of molecular processes, beyond conventional MRI methods [37;38]. However, the experimentally measured signal change may not be solely caused by relaxivity change, but also vary with contrast agent concentration. Hence, for molecular imaging, contrast agent’s concentration has to be determined first. Although this is not a problem for *in vitro* test, it becomes quite challenging for *in vivo* applications, in that MR probe concentration is often dynamic, heterogeneous and generally not known exactly. Hence, it is beneficial to delineate both the contrast agent concentration and exchange properties from a single experiment, for which, we believe the proposed RFP CEST MRI may serve as a very helpful alternative.

It is important to compare the proposed RFP CEST MRI with several published articles that also studied the RF power dependence nature of CEST MRI [25–28]. Previously, we derived the empirical solution to describe the RF power-dependent nature of CEST MRI [26]. That study, however, did not attempt to elucidate the dependence of optimal RF power on exchange property and labile proton concentration. A subsequent study of ours showed that spillover effects can be taken into account iteratively, allowing chemical exchange rate hence, pH, to be calibrated from CEST MRI [25]. In that study, however, we had to first determine labile proton concentration in order to derive pH. In addition, the work of McMahon et al. showed that numerical fitting can also be utilized to quantify exchange rate in CEST agents using saturation time and power (QUEST and QUESP) [27]. By comparison, our current study showed that by identifying a single RF power, optimal RF power, the underlying CEST system can be reasonably quantified. As such, the total scan time can be minimized if the optimal RF power can be obtained by interpolating CEST MRI contrast of several RF powers, provided that the typical range of exchange rate is known.

It is also necessary to point out several potential limitations of the proposed technique. Because exchange rate and labile proton content are derived from optimal RF power, it is very important to have homogeneous magnetic field (both B_0 and B_1), particularly so if per voxel analysis is needed [28]. Whereas perfect field homogeneity can hardly be achieved, several field inhomogeneity correction algorithms have been developed and may be applied to reduce measurement errors [28;39]. We also showed that RFP CEST MRI moderately depends on the bulk water relaxation rate, while it has negligible dependence on labile proton relaxation

constants. This is fortunate because the bulk water relaxation rate can be reasonably estimated or measured experimentally. In fact, for certain applications of CEST MRI such as acute stroke imaging, there is negligible change in bulk water relaxation rate, which may facilitate *in vivo* translation of quantitative RFP CEST MRI [22;31]. In addition, it is also important to note that the estimated exchange rate is slightly overestimated, which leads to an underestimation of labile proton concentration. This occurs because we used a simplified equation (Eq. 2) to derive exchange rate from optimal RF power, while numerical simulation or Eq. 1 can be used instead to improve the precision. Nevertheless, Eq. 2 provides a fast estimation of the exchange rate, which, if necessary, can be used as an initial guess for numerical fitting. Moreover, our results showed that the optimal RF power increases sub-linearly with exchange rate (Fig. 3 and fig 4). Hence, for imaging of CEST agents of high exchange rates, a large change in exchange rate may only elicit a moderate difference in optimal RF power. As a result, the precision of the proposed RFP CEST MRI technique may be limited. However, such a limit can be partially offset by conducting experiments at higher magnetic field, because higher chemical offset offers an increased dynamic range of optimal RF power (Fig. 3 a) [35]. While on the other hand, for extremely fast exchange rates such as those of paramagnetic CEST agents (PARACEST), optimal RF power may not be obtainable due to specific absorption rate (SAR) limit, and alternative data analysis methods such as QUESP and direct numerical fitting may have to be used instead [27;34;40].

6. CONCLUSIONS

In this work, we demonstrated that the RF power (RFP) dependence of CEST MRI can be used to simultaneously determine exchange rate and labile proton concentration. In particular, optimal RF power, at which CEST MRI contrast reaches its maximum, varies strongly with exchange rate but has minimal dependence on the labile proton concentration. As such, optimal RF power may serve as a useful parameter for quantitative characterization of the underlying CEST system, complementing the commonly used apparent CEST MRI method. The theoretical derivation was confirmed by numerical simulation, and further experimental validation is needed to evaluate the practicality and sensitivity of the proposed technique.

Acknowledgments

This study was supported in part by grants from AHA/SDG 0835384N and NIH/NINDS R21NS061119-01. The author would like to thank Dr. Peter Caravan for stimulating discussions.

REFERENCES

1. Forsen S, Hoffman RA. Study of moderately rapid chemical exchange reactions by means of nuclear magnetic double resonance. J. Chem. Phys 1963;39:2892–2901.
2. Wolff SD, Balaban RS. NMR imaging of labile proton exchange. J. Magn. Reson 1990;86:164–169.
3. Ward KM, Aletras AH, Balaban RS. A new class of contrast agents for MRI based on proton chemical exchange dependent saturation transfer (CEST). J. Magn. Reson 2000;143:79–87. [PubMed: 10698648]
4. Aime S, Delli Castelli D, Fedeli F, Terreno E. A paramagnetic MRI-CEST agent responsive to lactate concentration. J Am Chem Soc 2002;124:9364–9365. [PubMed: 12167018]
5. Snoussi K, Bulte JWM, Gueron M, van Zijl PCM. Sensitive CEST agents based on nucleic acid imino proton exchange: detection of poly(rU) and of a dendrimer-poly(rU) model for nucleic acid delivery and pharmacology. Magn. Reson. Med 2003;49:998–1005. [PubMed: 12768576]
6. Zhang S, Merritt M, Woessner D, Lenkinski R, Sherry A. PARACEST agents: modulating MRI contrast via water proton exchange. Acc Chem Res 2003;36:783–790. [PubMed: 14567712]
7. Wu Y, Zhou Y, Ouari O, Woods M, Zhao P, Soesbe TC, Kiefer GE, Sherry AD. Polymeric PARACEST Agents for Enhancing MRI Contrast Sensitivity. Journal of the American Chemical Society 2008;130:13854–13855. [PubMed: 18817395]

8. Zhang S, Trokowski R, Sherry AD. A Paramagnetic CEST Agent for Imaging Glucose by MRI. J. Am. Chem. Soc 2003;125:15288–15289. [PubMed: 14664562]
9. van Zijl PCM, Jones CK, Ren J, Malloy CR, Sherry AD. MRI detection of glycogen in vivo by using chemical exchange saturation transfer imaging (glycoCEST). Proc Natl Acad Sci 2007;104:4359–4364. [PubMed: 17360529]
10. Gilad AA, McMahon MT, Walczak P, Winnard PT, Raman V, van Laarhoven HWM, Skoglund CM, Bulte JWM, van Zijl PCM. Artificial reporter gene providing MRI contrast based on proton exchange. Nat Biotech 2007;25:217–219.
11. Yoo B, Raam MS, Rosenblum RM, Pagel MD. Enzyme-responsive PARACEST MRI contrast agents: a new biomedical imaging approach for studies of the proteasome. Contrast Media Mol Imaging 2007;2:189–198. [PubMed: 17712869]
12. Vasalatiy O, Gerard RD, Zhao P, Sun X, Sherry AD. Labeling of Adenovirus Particles with PARACEST Agents. Bioconjug Chem 2008;19:598–606. [PubMed: 18254605]
13. Aime S, Castelli DD, Crich SG, Gianolio E, Terreno E. Pushing the Sensitivity Envelope of Lanthanide-Based Magnetic Resonance Imaging (MRI) Contrast Agents for Molecular Imaging Applications. Accounts of Chemical Research 2009;42:822–831. [PubMed: 19534516]
14. Aime S, Carrera C, Castelli DD, Crich SG, Terreno E. Tunable Imaging of Cells Labeled with MRI-PARACEST Agents. Angew Chem Int Ed Engl 2005;44:1813–1815. [PubMed: 15723362]
15. Weissleder R, Cheng H, Bogdanova A, Bogdanov AJ. Magnetically labeled cells can be detected by MR imaging. J Magn Reson Imaging 1997;7:258–263. [PubMed: 9039625]
16. Anna M, Phillip Zhe S, David C, Dagmar H, Ralph W, Myra AL. MRI of insulitis in autoimmune diabetes. Magn Reson Med 2002;47:751–758. [PubMed: 11948737]
17. A, Gilad; A; van Laarhoven, H.; M, W.; McMahon, M.; T; Walczak, P.; Heerschap, A.; Neeman, M.; van Zijl, P.; M, C.; Bulte, J.; M, W. Feasibility of concurrent dual contrast enhancement using CEST contrast agents and superparamagnetic iron oxide particles. Magn Reson Med 2009;61:970–974. [PubMed: 19189296]
18. Kraitchman DL, Bulte JWM. In Vivo Imaging of Stem Cells and Beta Cells Using Direct Cell Labeling and Reporter Gene Methods. Arterioscler Thromb Vasc Biol 2009;29:1025–1030. [PubMed: 19359666]
19. McMahon MT, Gilad AA, DeLiso MA, Berman S, Bulte JW, van Zijl PC. New “Multi-Color” Polypeptide DIACEST Contrast Agents for MR Imaging. magn Reson Med. 2008 in press.
20. Zhou J, Lal B, Wilson DA, Laterra J, van Zijl PCM. Amide proton transfer (APT) contrast for imaging of brain tumors. Magn. Reson. Med 2003;50:1120–1126. [PubMed: 14648559]
21. Zhou J, Payen J, Wilson DA, Traystman RJ, van Zijl PCM. Using the amide proton signals of intracellular proteins and peptides to detect pH effects in MRI. Nature Med 2003;9:1085–1090. [PubMed: 12872167]
22. Sun PZ, Zhou J, Sun W, Huang J, van Zijl PCM. Detection of the ischemic penumbra using pH-weighted MRI. J Cereb Blood Flow Metab 2007;27:1129–1136. [PubMed: 17133226]
23. Ward KM, Balaban RS. Determination of pH using water protons and chemical exchange dependent saturation transfer (CEST). Magn. Reson. Med 2000;44:799–802. [PubMed: 11064415]
24. Ali MM, Liu G, Shah T, Flask CA, Pagel MD. Using Two Chemical Exchange Saturation Transfer Magnetic Resonance Imaging Contrast Agents for Molecular Imaging Studies. Accounts of Chemical Research 2009;42:915–924. [PubMed: 19514717]
25. Sun PZ, Sorensen AG. Imaging pH using the Chemical Exchange Saturation Transfer (CEST) MRI: Correction of Concomitant RF Irradiation Effects to Quantify CEST MRI for Chemical Exchange Rate and pH. Magn Reson Med 2008;60:390–397. [PubMed: 18666128]
26. Sun PZ, van Zijl PCM, Zhou J. Optimization of the irradiation power in chemical exchange dependent saturation transfer experiments. J Magn Reson 2005;175:193–200. [PubMed: 15893487]
27. McMahon M, Gilad A, Zhou J, Sun PZ, Bulte J, van Zijl PC. Quantifying exchange rates in chemical exchange saturation transfer agents using the saturation time and saturation power dependencies of the magnetization transfer effect on the magnetic resonance imaging signal (QUEST and QUESP): Ph calibration for poly-L-lysine and a starburst dendrimer. Magn Reson Med 2006;55:836–847. [PubMed: 16506187]

28. Sun PZ, Farrar CT, Sorensen AG. Correction for artifacts induced by B0 and B1 field inhomogeneities in pH-sensitive chemical exchange saturation transfer (CEST) imaging. Magn Reson Med 2007;58:1207–1215. [PubMed: 17969015]
29. Sun PZ, Zhou J, Huang J, van Zijl P. Simplified Quantitative Description of Amide Proton Transfer (APT) Imaging During Acute Ischemia. Magn Reson Med 2007;57:405–410. [PubMed: 17260362]
30. Salhotra A, Lal B, Laterra J, Sun PZ, van Zijl PCM, Zhou J. Amide proton transfer imaging of 9L gliosarcoma and human glioblastoma xenografts. NMR Biomed 2008;21:489–497. [PubMed: 17924591]
31. Jokivarsi KT, Gröhn HI, Gröhn OH, Kauppinen RA. Proton transfer ratio, lactate, and intracellular pH in acute cerebral ischemia. Magn Reson Med 2007;57:647–653. [PubMed: 17390356]
32. Jain RK, Duda DG, Willett CG, Sahani DV, Zhu AX, Loeffler JS, Batchelor TT, Sorensen AG. Biomarkers of response and resistance to antiangiogenic therapy. Nat Rev Clin Oncol 2009;6:327–338. [PubMed: 19483739]
33. Zhou J, Blakeley JO, Hua J, Kim M, Laterra J, Pomper MG, van Zijl PCM. Practical data acquisition method for human brain tumor amide proton transfer (APT) imaging. magn Reson Med 2008;60:842–849. [PubMed: 18816868]
34. Woessner DE, Zhang S, Merritt ME, Sherry AD. Numerical solution of the Bloch equations provides insights into the optimum design of PARACEST agents for MRI. Magn Reson Med 2005;53:790–799. [PubMed: 15799055]
35. Zhou J, Wilson DA, Sun PZ, Klaus JA, van Zijl PCM. Quantitative description of proton exchange processes between water and endogenous and exogenous agents for WEX, CEST, and APT experiments. Magn. Reson. Med 2004;51:945–952. [PubMed: 15122676]
36. Baguet E, Roby C. Off-resonance irradiation effect in steady-state NMR saturation transfer. J. Magn. Reson 1997;128:149–160. [PubMed: 9356270]
37. Garcia-Martin M, L, Martinez GV, Raghunand N, Sherry AD, Zhang S, Gillies R, J. High resolution pH(e) imaging of rat glioma using pH-dependent relaxivity. magn Reson Med 2006;55:309–315. [PubMed: 16402385]
38. Louie AY, Huber MM, Ahrens ET, Rothbacher U, Moats R, Jacobs RE, Fraser SE, Meade TJ. In vivo visualization of gene expression using magnetic resonance imaging. Nature Biot 2000;18:321–325.
39. Kim M, Gillen J, Landman BA, Zhou J, van Zijl PCM. Water saturation shift referencing (WASSR) for chemical exchange saturation transfer (CEST) experiments. Magn Reson Med 2009;61:1441–1450. [PubMed: 19358232]
40. Li AX, Hudson RHE, Barrett JW, Johns CK, Pasternak SH, Bartha R. Four-pool modeling of proton exchange processes in biological systems in the presence of MRI-paramagnetic chemical exchange saturation transfer (PARACEST) agents. Magn Reson Med 2008;60:1197–1206. [PubMed: 18958857]

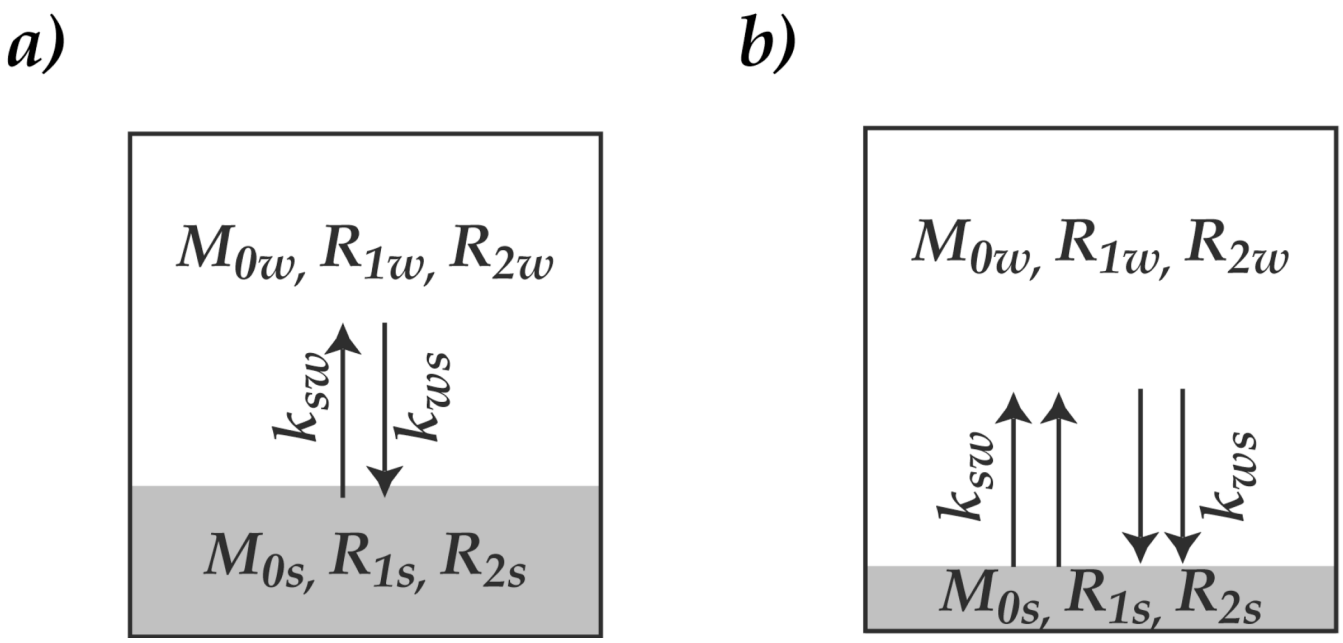

Fig. 1.
Illustration of two representative CEST systems, a) 2-pool exchange model that depicts relatively concentrated CEST agents undergoing slow chemical exchange, b) shows the case of dilute CEST agents undergoing faster interaction with bulk water.

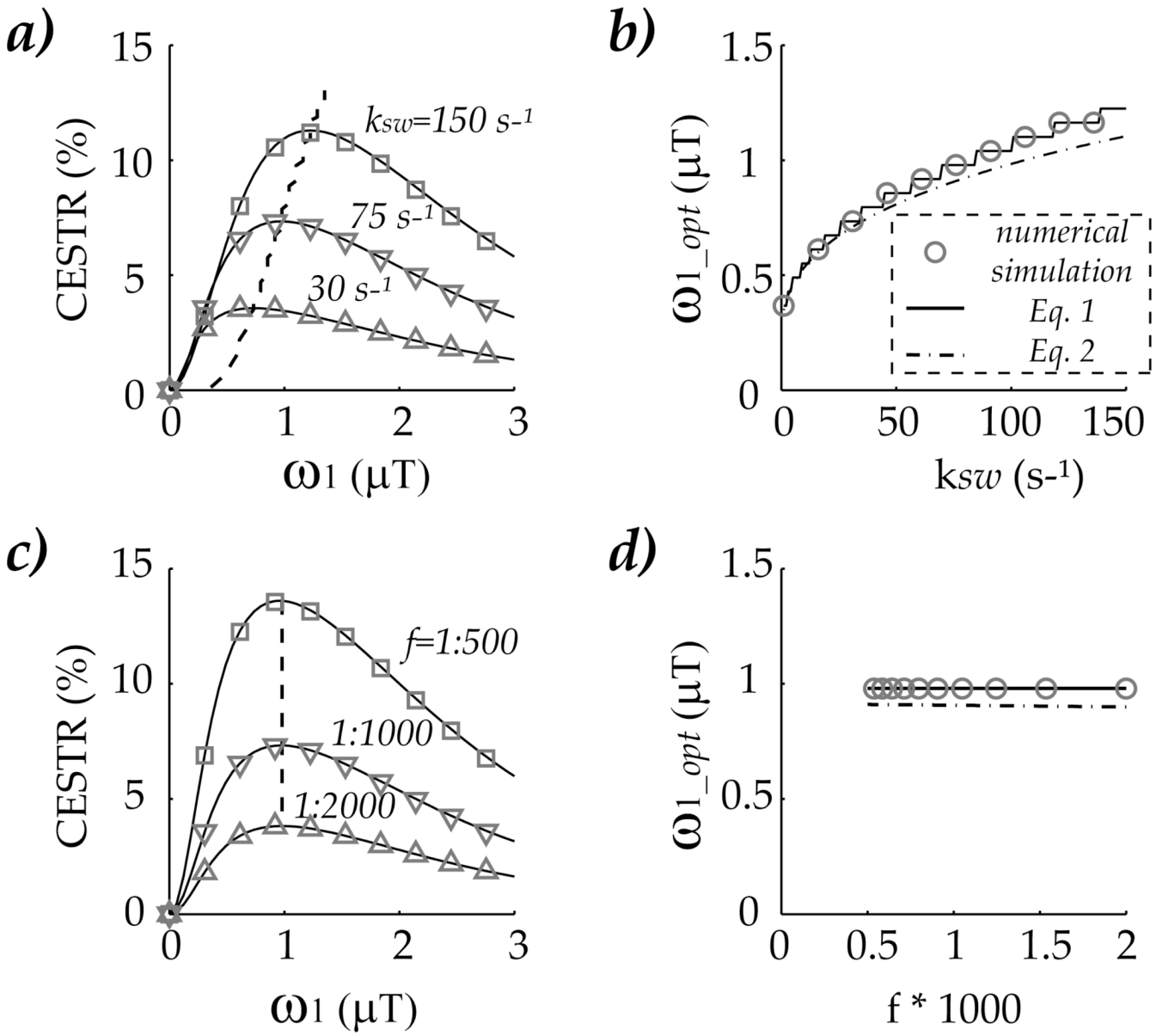

Fig. 2.

a) CEST MRI contrast was simulated as a function RF power for three exchange rates, 30, 75 and 150 s^{-1} at a labile proton content of 1:1000. The up triangle, down triangle and square markers denote numerical simulation, while the line represent empirical solution results using Eq. 1, which agreed well. The optimal RF power for each exchange rate is shown in dashed line, b) The Optimal RF power was plotted as a function of exchange rate, with circles, sold line and dashed line represent numerically simulated results, analytical estimates from Eq. 1 and Eq. 2, respectively. In addition, CEST MRI was also simulated for labile proton concentration effect, in which concentration was varied from 1:2000 (up triangle), 1:1000 (down triangle) to 1:500 (square) for a representative exchange rate of 75 s^{-1} in (*c*), with the optimal RF power shown in the dashed line, d) The optimal RF power estimated from empirical solution of Eq. 1 and Eq. 2 agrees well with the numerical simulation (circle).

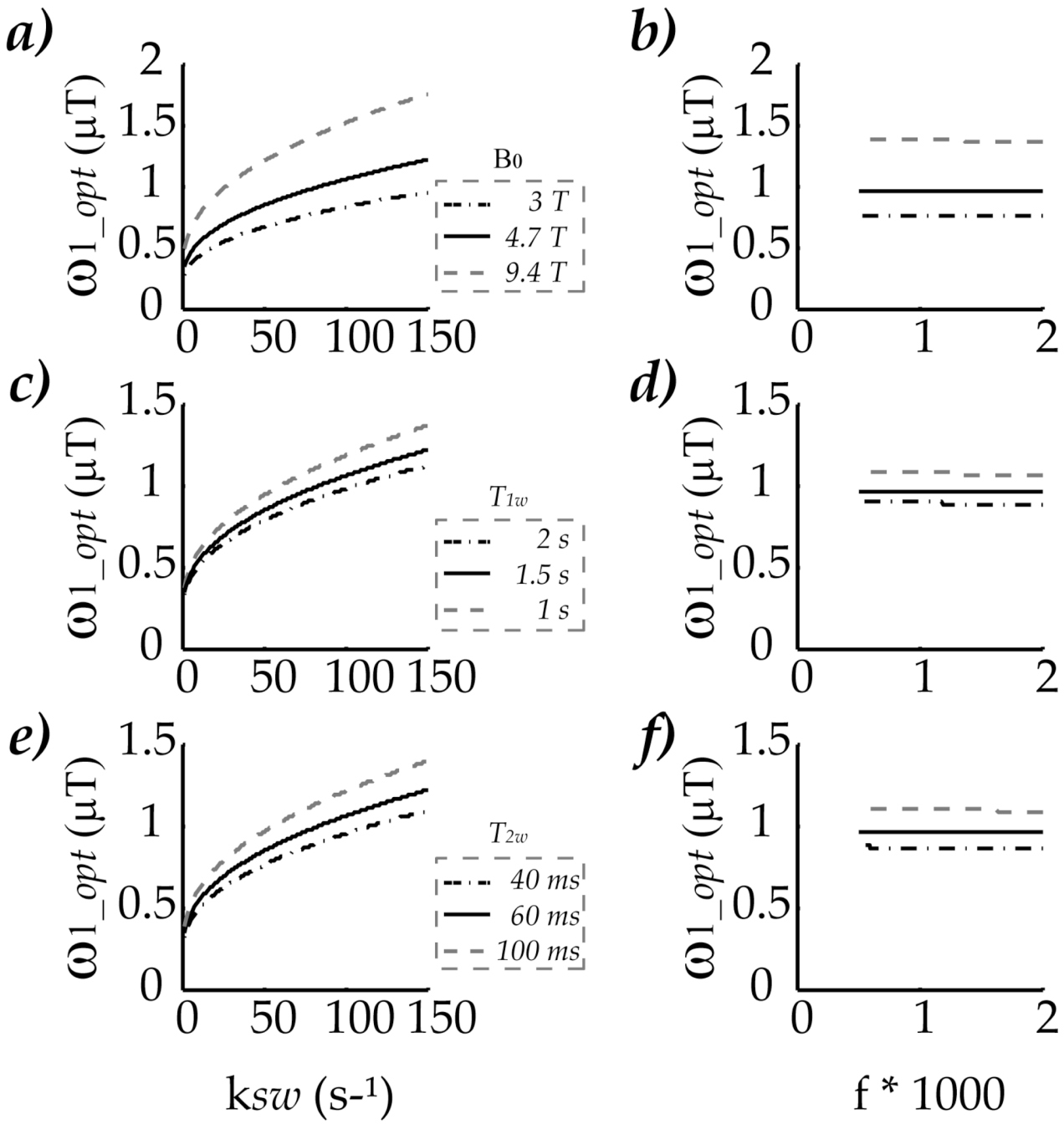

Fig. 3.

evaluation of the dependence of optimal RF power upon chemical offset and relaxation rates for the case of dominant change in exchange rate (Figs 3a, c and d) and the case of labile proton concentration effect (Figs 3b, d and f). Specifically, Figs 3a and b compared optimal RF power as a function of exchange rate and labile proton concentration for amide proton at field strength of 3,4.7 and 7T, respectively. It showed although optimal RF power increases with chemical offset, the optimal RF power remains constant for the range of investigated labile proton concentration, while it increases with exchange rate. In addition, Figs 3c and d evaluated optimal RF power when T_{1w} was varied from 1,1.5 to 2 s, while Figs. 3e and f studied bulk water T_{2w} dependence from 40, 60 to 100 ms. All simulation showed that for a given set

parameters of chemical offset and relaxation rates, the optimal RF power depends on exchange rate, with negligible dependence on the labile proton concentration, in reasonable agreement with theoretical prediction.

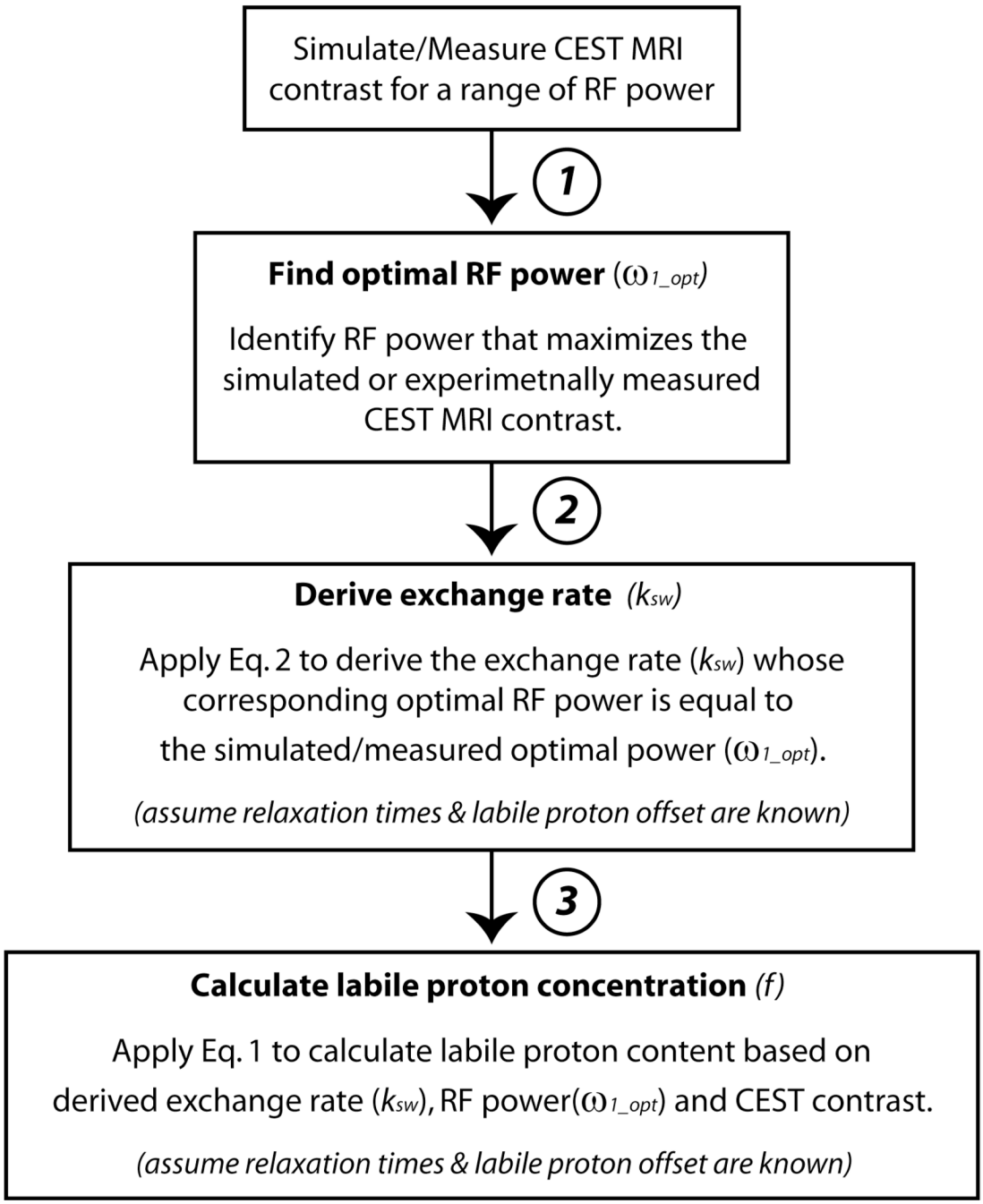

Fig. 4.

a flow chart that describes the proposed quantitative RFP-CEST MRI technique. Step 1) CEST MRI contrast is simulated or experimentally measured for a range of RF power. 2) Optimal RF power is identified by finding the RF power that maximizes CEST MRI contrast. 3) Exchange rate is estimated from optimal RF power using Eq. 2, provided that relaxation parameters and chemical offsets are known. 4) Labile proton concentration is derived from Eq. 1, provided that relaxation rates, RF offsets are known.

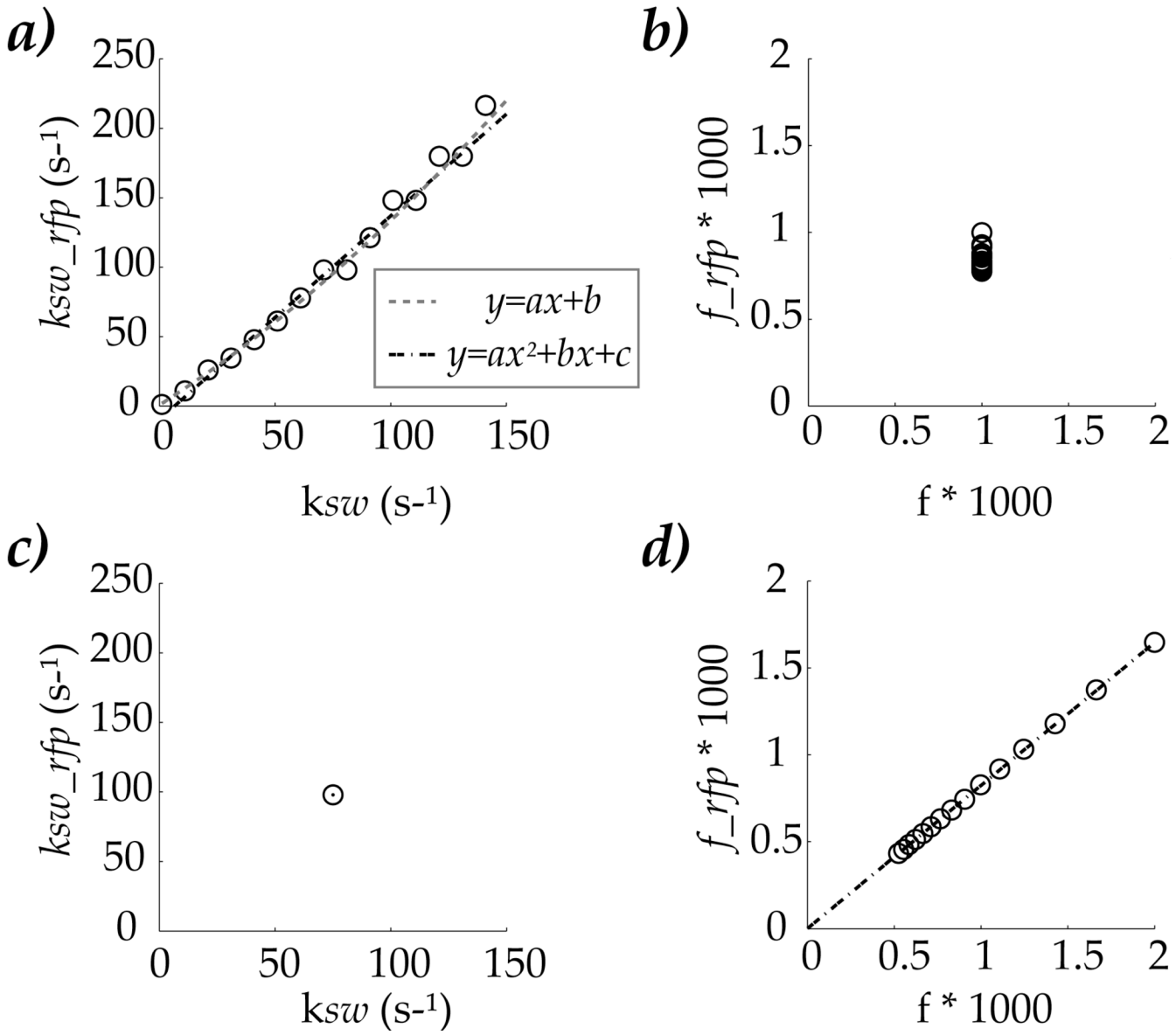

Fig. 5.

Evaluation of the inverse problem that whether exchange rate and labile proton concentration effect can be simultaneously determined from the optimal RF power. For the first case, exchange rate was varied between 1 and 150 s^{-1}, while the labile proton concentration was 1:1000. The estimated exchange rate correlated well with simulated values (a), and can be described by a linear function. In addition, the derived labile proton concentration had a narrow distribution from the simulated value of 1:1000 (b). For the second case, labile proton concentration was varied from 1:2000 to 1:500, for a representative exchange rate of 75 s^{-1}. The exchange rate was found to be 98 s^{-1} from Eq. 2, in contrast to simulated value of 75 s^{-1}(c). Moreover, the estimated labile proton concentration vs. simulated value can be described by a linear function.